JOURNAL OF MATERIALS SCIENCE 18 (1983) 1810–1826

A tensile testing technique for fibre-reinforced composites at impact rates of strain

J. HARDING, L. M. WELSH
Department of Engineering Science, University of Oxford, Parks Road, Oxford, UK

A brief review is given of techniques which have been employed in attempts to determine the mechanical properties of composite materials under tensile impact loading. The difficulties encountered in the design of a satisfactory tensile impact testing machine for composite materials are discussed and a new method, using a modified version of the standard tensile split Hopkinson's pressure bar (SHPB), is described. Dynamic stress–strain curves for unidirectionally-reinforced carbon/epoxy composite, in which failure occurs in less than 30 μsec at a mean strain rate of about 400 sec^{-1}, are presented and their validity is established. An extension of the technique to allow the testing of woven-roving reinforced glass/epoxy composites is described and dynamic stress–strain curves obtained for which the times to failure approach 100 μsec and the average strain rate is of the order of 1000 sec^{-1}. Comparative stress–strain curves at low and intermediate rates of strain are obtained and the effect of strain rate, over about 7 orders of magnitude, on the tensile modulus, and strength, fracture strain and energy absorbed in fracturing is determined. The limitations of the technique are discussed.

1. Introduction

The need for a full characterization of the behaviour of fibre-reinforced composites under dynamic loading conditions has prompted numerous investigations in recent years [1–3]. Nevertheless, because of the experimental difficulties involved few reliable data are available. Much of the work that has been done has employed the instrumented Charpy test in which a notched beam specimen is subjected to impact bending [4, 5]. Although load–time records obtained from the instrumented tup may be used to estimate the energy absorbed in the various stages of the fracturing process, stress wave reflections and the complex geometry of the specimen inhibit any fundamental analysis of the material response and its dependence on loading rate [6]. A need for the development of tests covering a wide range of loading rates, up to impact, in uniaxial tension and compression and in pure shear has been clear for some time [7] and has recently been restated [6].

For isotropic materials, tests at the highest rates of loading are frequently performed using the split Hopkinson's pressure bar (SHPB) technique. In recent years this technique has been adapted to the testing of composite materials in compression [8, 9] and torsion [10] while a high-speed punch version of the SHPB has been used [11] to determine the resistance to dynamic perforation.

The greatest difficulty has been experienced, however, in obtaining reliable data for impact tension. Tensile strain rates of about 10 sec^{-1} have been obtained in an apparatus using a gas-driven piston [12] while rates approaching 500 sec^{-1} were achieved when an explosive charge was used to drive the impacting head [2]. In both cases high-speed photographic techniques were required to monitor the strain and, in the latter investigation, slipping at the clamps was a major problem. Drop-weight techniques have been used by several investigators [13, 14], strain being determined from strain gauges attached directly to the specimen. This method of strain measurement is very accurate up to the point at which the gauges fail but is unsatisfactory for materials which exhibit surface damage prior to failure. It

0022–2461/83 $03.00 + .12

is also clear that the drop-weight technique, as developed in these investigations, is not free of stress wave reflections in the load cell [3]. These are superimposed on the specimen stress–time response.

Some of the difficulties have been overcome in a technique proposed by Daniel *et al.* [15] where the specimen, in the form of a ring or shell, is loaded by means of an internal pressure pulse. In theory the specimen is stressed uniformly at all times so stress wave reflections do not arise and problems associated with end effects and the fixing of the specimen to the loading bars are eliminated. Nevertheless several major disadvantages remain. The specimen experiences a continuously decreasing strain rate throughout the test. The state of stress in the ring specimen is far from simple including, as well as membrane stresses, a pressure induced radial stress at the inside face and shear stresses resulting from any variation in the dynamic load along the axial direction. Also, the practical difficulty of making the specimens and actually performing the tests limits its value as a technique for the rapid evaluation of a large number of materials.

The only previous application of the Hopkinson bar technique to impact tension testing of composites is in the work of Kawata *et al.* [16]. In their machine, which works on the bar-block principle, a cylindrical tensile specimen with a screw fixing is used. Accurately coaxial impact is required on the impact block to minimize bending stresses in the specimen. Three different techniques are used to determine the velocity of the block, which is assumed also to be that of the impact end of the specimen gauge section. However, in view of the low values of strain being measured and the lack of an independent check, some doubt must remain regarding the accuracy of the resulting strain determination.

Very recently another tensile impact test [17] using the Hopkinson bar technique has been successfully developed at Oxford. The specimen design closely follows the proposals of Ewins [18], which have gained widespread acceptance for the quasi-static tension testing of composite materials [19]. The testing technique is similar to that used in the testing of isotropic materials [20] but incorporates an instrumented loading, or input, bar. Stress equilibrium across the specimen is achieved early in the test and good agreement is obtained between the measurements of elastic strain determined from strain gauges mounted on the specimen and those determined from the Hopkinson-bar analysis.

The present paper describes the development and validation of this technique and its application to the tensile impact testing of uniaxially-reinforced carbon fibre/epoxy composite. The behaviour observed is compared with that found in tests performed at lower rates. The technique is then extended to allow the testing of woven-roving reinforced glass fibre/epoxy composite where the strains to fracture are as much as a factor of 10 greater than for the CFRP (carbon fibre reinforced plastic) material and results are presented for tests on two orientations of specimen at rates from quasi-static to about 1000 sec^{-1}.

2. Experimental details

In the original compression version of the Hopkinson-bar the specimen is sandwiched between two elastic loading bars and the incident, reflected and transmitted stress waves are determined from strain gauges attached to these loading bars on either side of the specimen. In the standard tensile version of the apparatus [20] the input loading bar becomes the weighbar tube within which the output, or inertia, bar slides freely, the specimen connecting the two at the yoke, see Fig. 1a. In a specimen test strain gauges on the inertia bar monitor the transmitted stress wave. To determine the input conditions, however, a separate "elastic" test is required, performed under identical impact conditions but with the specimen and the inertia bar replaced by an elastic bar. For tests on ductile metal specimens this enables the dynamic plastic strain and strain rate to be determined with reasonable accuracy using specimens of a gauge length short enough for the attainment of stress equilibrium across the specimen to be assumed from an early stage in the test. This technique does not, however, allow for an accurate determination of strain during the elastic deformation of the specimen.

When applied to composite materials several major problems arise. Because of the difficulty of ensuring a tensile failure in the gauge section rather than a shear failure in the grips and because of the need to minimize stress concentrations associated with the anisotropic nature of the material, significantly longer test specimens are required, making the attainment of stress equilibrium across the specimen more difficult. In

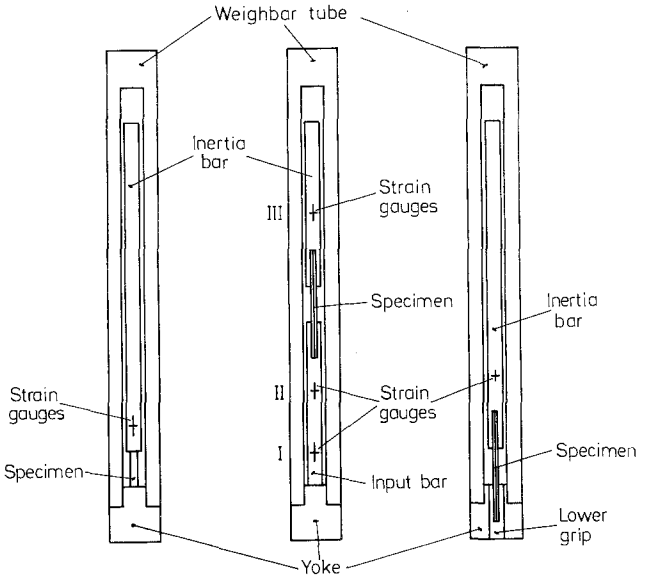

Figure 1 Schematic arrangement of tensile Hopkinson bar. (a) Standard version, (b) modified version for testing CFRP, and (c) modified version for testing GFRP.

addition, since for most composite materials the total strain to failure is only a small fraction of that obtained in metal specimens, the accurate determination of strain becomes very much more critical.

For these reasons the standard tensile version of the split Hopkinson's pressure bar was modified, see Fig. 1b, to include an instrumented input bar preceding the specimen and inertia bar and also sliding freely within the weighbar tube. Strain gauges at two stations on the input bar enable the incident and reflected waves to be monitored in the specimen test itself. Thus the validity of the assumption of stress equilibrium across the specimen may be directly checked and strain determination in the specimen may be made from measurements taken in a single test, eliminating the need to compare results from two potentially slightly different tests.

Within the constraints of the existing weighbar tube, however, the introduction of the input bar limits the maximum length of the inertia bar and hence the maximum duration of test for which the full dynamic analysis is possible. As is apparent from Fig. 2, which shows the Lagrange diagram for the modified tensile Hopkinson bar, the time interval over which the wave analysis in the input bar can be carried out cannot conveniently exceed $(T_2 - T_1)$. Since in the present apparatus $T_2 \simeq 55\,\mu$sec and $T_1 \simeq 25\,\mu$sec it is necessary that the specimen should fracture within about $30\,\mu$sec. In practice this limits the application of the technique to uniaxially-reinforced CFRP and initial results will be presented for specimens of this material.

3. Specimen details

Unidirectionally-reinforced carbon/epoxy specimens having the dimensions shown in Fig. 3a were cut with the tensile axis parallel to the direction of

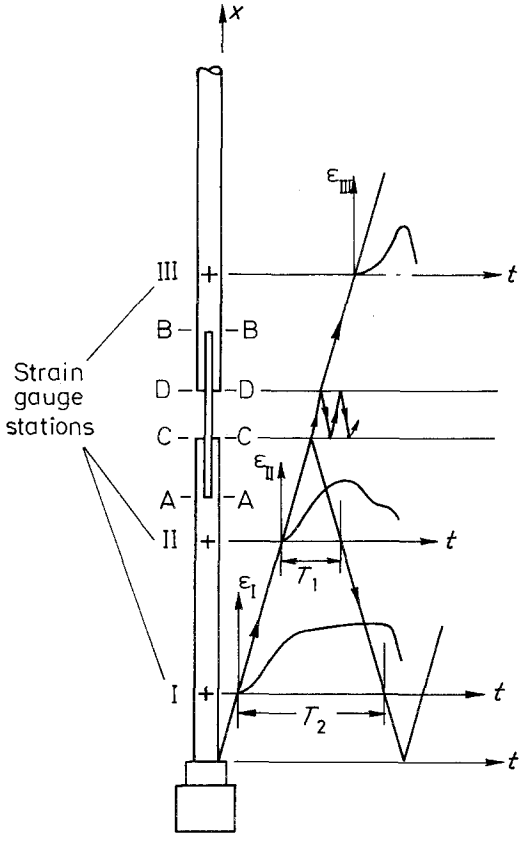

Figure 2 Lagrange (x, t) diagram for modified tensile Hopkinson bar.

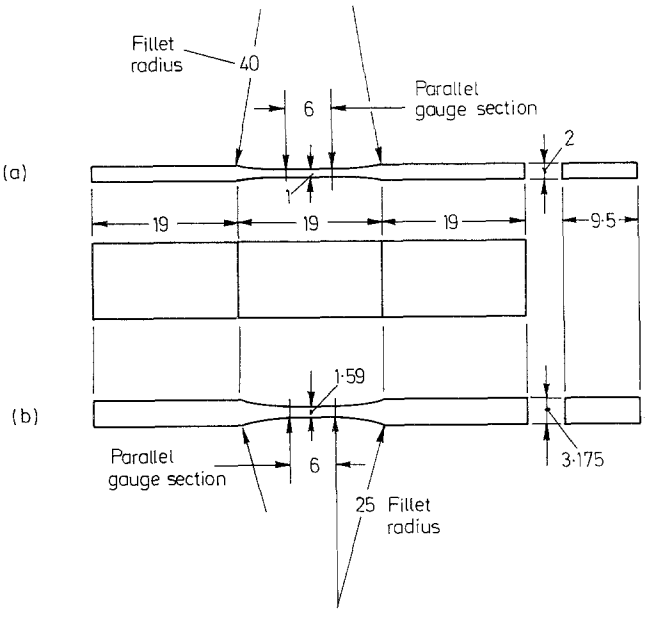

Figure 3 Specimen design (all dimensions in mm) (a) CFRP and (b) GFRP.

reinforcement from 2 mm plate supplied by Bristol Composite Materials Ltd. The fibres were of type HYFIL-Torayca-130-S in a proprietary resin system of type R7H, a modified bisphenol A medium temperature epoxy similar to Araldite MY750. A typical quasi-static tensile strength of 1.2 GPa and a tensile modulus of 131 GPa were quoted by the manufacturer for a composite volume fraction of 60%. The parallel grip regions of the specimen were fixed into parallel-sided slots in the loading bars using Chemlok 304 high-strength epoxy adhesive. With a grip region of length 19 mm tensile failure was obtained in the specimen gauge region before shear failure occurred in the adhesive. Because of the relatively long grip section it was anticipated that problems might arise from stress wave reflections at the sections AA and BB in Fig. 2. In practice, however, the change in impedance across these sections was so slight that any reflections resulting were too small to be detected.

In subsequent tests on commercially produced (high volume fraction) unidirectionally-reinforced glass/epoxy specimens, however, failure was always found to occur by shear within the specimen at the resin/fibre interface closest to the adhesive in the loading-bar slots. For tests on GFRP (glass fibre reinforced plastics), therefore, a woven-roving reinforced material was used. Specimens having the dimensions shown in Fig. 3b were cut from 1/8 inch thick plate of "Permaglass 22FE" supplied by Permali Ltd., incorporating 9 mats of Marglass 116S fine-woven fibres in an Araldite epoxy matrix of MY753 resin and HY951 hardener. Specimens were cut with the tensile axis either parallel to one of the principal reinforcing directions, 0° specimens, or lying in the plane of reinforcement and inclined at 45° to both the principal reinforcing directions, 45° specimens.

As an additional check on the Hopkinson bar analysis for strain and strain rate, some tests were performed with a further set of strain gauges attached directly to the gauge section of the specimen. Techni Measure 120 Ω strain gauges, type FL3A, having an active gauge region of 3 mm long by 1.9 mm wide, were bonded centrally on each face of the parallel central region of the specimen, using the recommended cyanoacrylate adhesive.

4. Validation of the impact testing technique

A typical set of strain–time traces for a test in which additional calibration gauges were attached directly to the specimen is shown in Fig. 4a. The small perturbation, which is regularly observed in such tests near the start of the transmitted strain–time trace, ϵ_{III}, coincides in time with the breakdown of the specimen gauges, ϵ_s, shortly before the specimen fractures. It is thought to be due to some resulting electrical interference. In tests where no gauges are attached directly to the specimen, see Fig. 4b, no such perturbation is observed. From the Lagrange diagram of Fig. 2 it may be

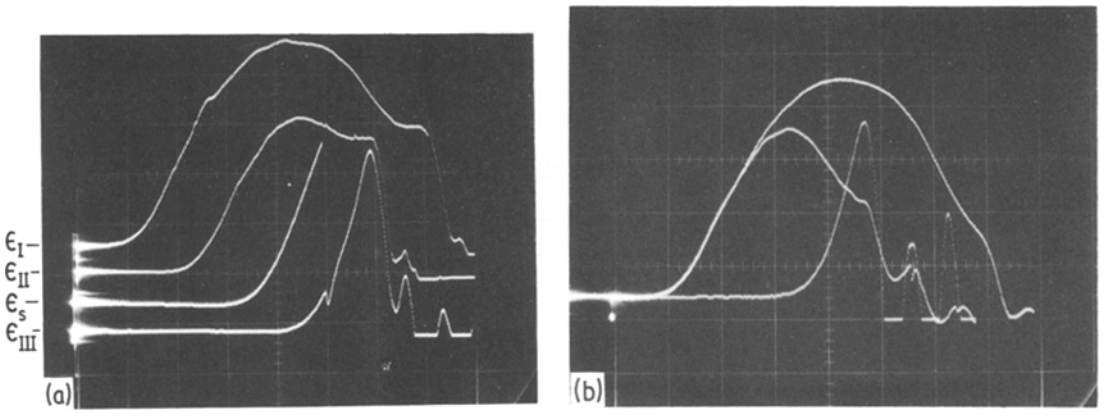

Figure 4 Strain-time traces for impact tests on CFRP (Total sweep time: 100 μsec). (a) With strain gauges attached to specimen. Strain–time signals from: ϵ_I – gauge position I; ϵ_{II} – gauge position II; ϵ_s – specimen gauges; ϵ_{III} – gauge position III. (b) With signals from gauge positions I and II superimposed.

seen that, in the absence of dispersion and for times $\leqslant T_1$ identical signals should be recorded at stations I and II. This is confirmed in Fig. 4b where it is shown that these two signals may be superimposed almost exactly for times up to about 25 μsec. Standard strain gauge bridges and two dual-channel transient recorders were used to store the strain–time traces of Fig. 4. These were then subsequently displayed and photographed on an oscilloscope screen while for calculation purposes a hard copy could be produced on a chart recorder.

Data obtained in this way was used in the Hopkinson-bar analysis, illustrated in Fig. 5, for a test on a CFRP specimen impacted at a velocity of about 10 m sec^{-1}. Again the strain–time traces from the two sets of input bar gauges are seen to superimpose almost exactly for times up to about 25 μsec. The subsequent difference between these two traces is used to determine the velocity and stress at the input end of the specimen, section CC in Fig. 2. The corresponding stress and velocity trace for the output end of the specimen, section DD in Fig. 2, derived from the inertia bar gauges, is delayed by just over 2 μsec, the time for an elastic wave to travel between sections CC and DD in a CFRP specimen. The stress–time traces for the two ends of the specimen, σ_{cc} and $E\epsilon_{III}$, are seen to coincide very closely almost from the start of loading, confirming the validity of the assumption of stress equilibrium across the specimen.

The corresponding strain is obtained by integrating between the velocity time curves for the two ends of the specimen in the usual way, giving the stress–strain curve of Fig. 6a. The specimen fails after about 25 μsec at a stress of 1.27 GPa and a strain, related to the gauge length of 19 mm, i.e. from CC to DD in Fig. 2, of about 0.9%. The average strain rate was about 350 sec. The stress–strain curve shows an initial linear region, corresponding to a modulus of 142 GPa, followed by a slight increase in stiffness preceding failure. Also shown, in Fig. 6b, is the stress–strain curve for the same test but with strain measurements obtained from the gauges attached directly to the specimen and relating, therefore, to the deformation in the

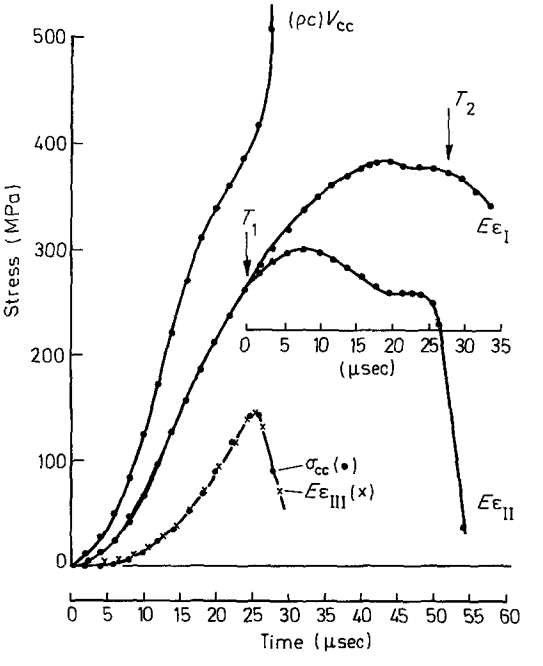

Figure 5 Hopkinson-bar analysis for impact test on CFRP.

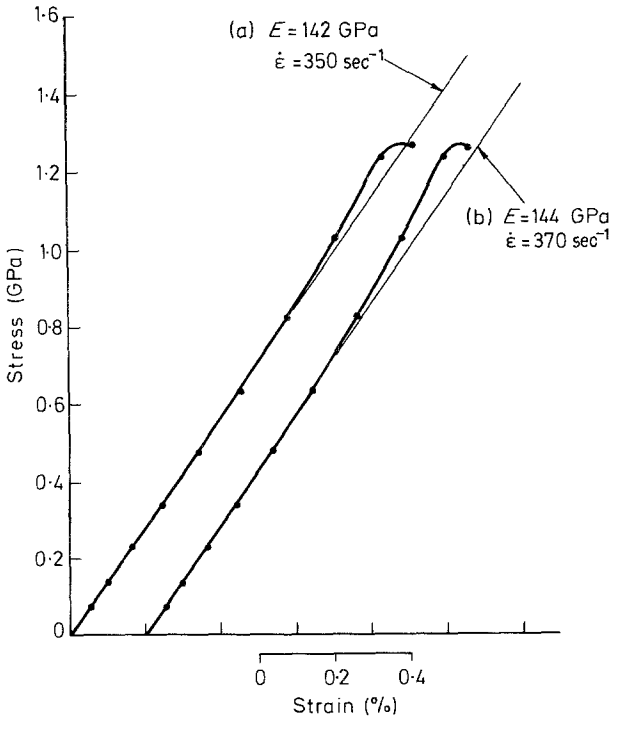

Figure 6 Tensile stress–strain curve for impact on CFRP at 10 msec^{-1}. (a) Specimen strain determined by Hopkinson-bar analysis. (b) Specimen strain determined from strain gauges attached to specimen.

parallel section of the specimen, i.e. for a gauge length of 3 mm. The two curves are very closely similar. At all stress levels the specimen strain gauges indicate a marginally lower strain than that derived from the Hopkinson bar analysis giving, therefore, a slightly higher initial modulus, 144 GPa compared to 142 GPa. As might be expected, the specimen gauges break down slightly before the failure of the specimen, i.e. at 23 μsec and at a strain of 0.86% giving an average strain rate of about 370 sec. That a genuine tensile failure is obtained is demonstrated in Fig. 7 which, for a CFRP specimen impacted at 10 m sec^{-1}, shows the fracture path passing through the strain gauges in the central parallel region of the specimen.

5. Consideration of experimental accuracy

The close correlation between the two experimental curves of Fig. 6 encourages considerable confidence in the validity of the testing technique. Both curves, however, rely on the same stress–time data and on the same assumption of stress equilibrium across the specimen. The accuracy of stress measurement at the inertia bar gauges is estimated to be about ±2%, after making some allowance for dispersion and wave reflections in the grip section, DD to BB. The accuracy of the stress measurement on the input side is probably less good because of the need to take the difference between two transient signals after adjusting for the time difference between them. The validity of the check on stress equilibrium depends both

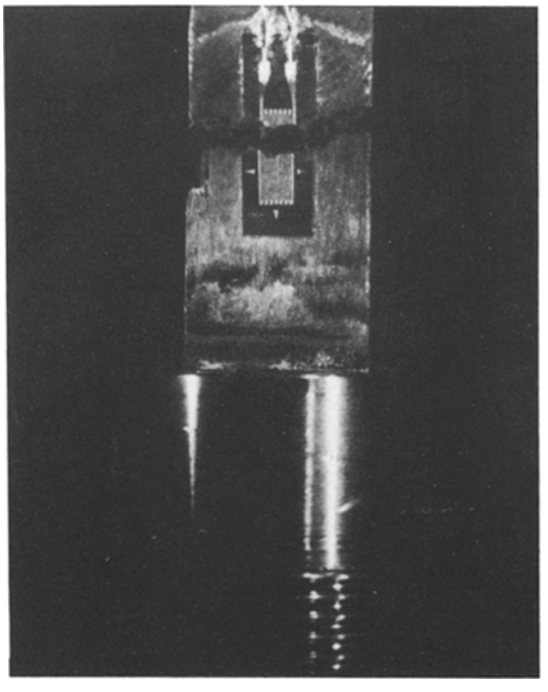

Figure 7 Tensile failure in parallel section of CFRP specimen with strain gauge attached.

on the accuracy of the stress measurement and also on the ability to identify with confidence the time zero's of the various transient signals. This confidence is strengthened by the use of transient recorders with a time resolution of 0.1 μsec which allows an accurate correlation to be made between the actual wave transit times between the various gauge stations and those predicted by elementary elastic wave theory. Since the specimen shows an essentially linear elastic behaviour this correlation may be carried through between gauge stations II and III. Allowance for a modified elastic wave speed in the grip regions, AA to CC and DD to BB, reduces the overall transit times by about 1.4 μsec. An error in the time measurement of this order corresponds to an error of about ±3% in the strain determined by the Hopkinson bar analysis. The stress–time signals for the two ends of the specimen may also be displaced relative to each other, affecting the validity of the assumed stress equilibrium and modifying slightly the average stress in the specimen at any given time. Taking all these effects together the maximum error in the modulus as determined by the Hopkinson bar analysis is estimated at ±7 GPa, i.e. about ±5%. A similar accuracy would be expected for the results based on strain measurements made from the specimen gauges.

6. Tests on GFRP material

The validity of the technique described above for the tensile impact testing of the CFRP composite has been demonstrated. Because of the high modulus and very low strains to fracture in CFRP specimens the accuracy of strain measurement was the most severe problem in these tests. Accuracy of the strain measurement is less critical in tests on GFRP specimens where the modulus is lower and the strains to fracture are higher. Other problems arise, however, since, in general, the time to fracture well exceeds 30 μsec and strain gauges attached directly to the specimen are of only limited use because the onset of surface damage leads to break down of the gauges well before the final fracture of the specimen. For these reasons an attempt was made to accurately calibrate the input signal on the standard tensile Hopkinson bar, Fig. 1c, using the known response of CFRP specimens, and then to use this test configuration for GFRP specimens so permitting a full dynamic analysis for times up to 150 μsec.

In the test configuration of Figs. 1b and 2 the velocity at the input end of the specimen, i.e. V_{cc} at section CC, is determined from the signals at gauge positions I and II. If the specimen can be treated as a thin elastic rod of known elastic constants, then an estimate of V_{cc} may also be derived from the signal at gauge position III, using the elementary theory of elastic wave propagation and calculating back through the specimen. These two estimates of V_{cc} are shown in Fig. 8 for a test at an impact velocity of 10 m sec^{-1} on CFRP material and are seen to be in close agreement for times up to about 16 μsec. At times greater than this the increase in stiffness of the specimen, as shown in Fig. 6, leads to a slight overestimate for V_{cc}, which is based on an assumed linear elastic response of the specimen. The reverse effect is observed when, at about 22 μsec, the specimen fractures, corresponding to a sudden drop in stiffness. It is clear, therefore, that a reasonably close estimate of the velocity on the input face of the specimen may be made from the strain–time trace on the output bar in an impact on CFRP material.

6.1. Calibration of the yoke velocity, V_y

In the light of this observation, an attempt was made to calibrate for the yoke velocity in the test configuration of Fig. 1c using the near-linear response obtained in a CFRP specimen test rather than by the standard calibration using a separate elastic bar. This has the important advantage that essentially the same yoke-specimen-inertia bar geometry is retained in both the calibration and the specimen tests. Strain gauges attached directly to the specimen were used to determine the strain in the specimen while the specimen stress was derived from the inertia bar gauge signal, assuming stress equilibrium across the specimen. The resulting dynamic stress–strain response, shown in Fig. 9a, was nearly identical to that shown in Fig. 6. The initial modulus was 145 GPa, the fracture stress 1285 MPa, the maximum strain 0.85% and the average strain rate about 350 sec^{-1}. Working back from the inertia bar strain–time signal, as described above, the input, or yoke, velocity, V_y, equivalent to V_{cc} in the test arrangement of Fig. 2, may be estimated. The velocity–time curve obtained for V_y differs slightly from that for V_{cc}, as might be expected since the details of the test arrangement are different. The difference in velocity is not sufficient, however, to significantly affect the dynamic

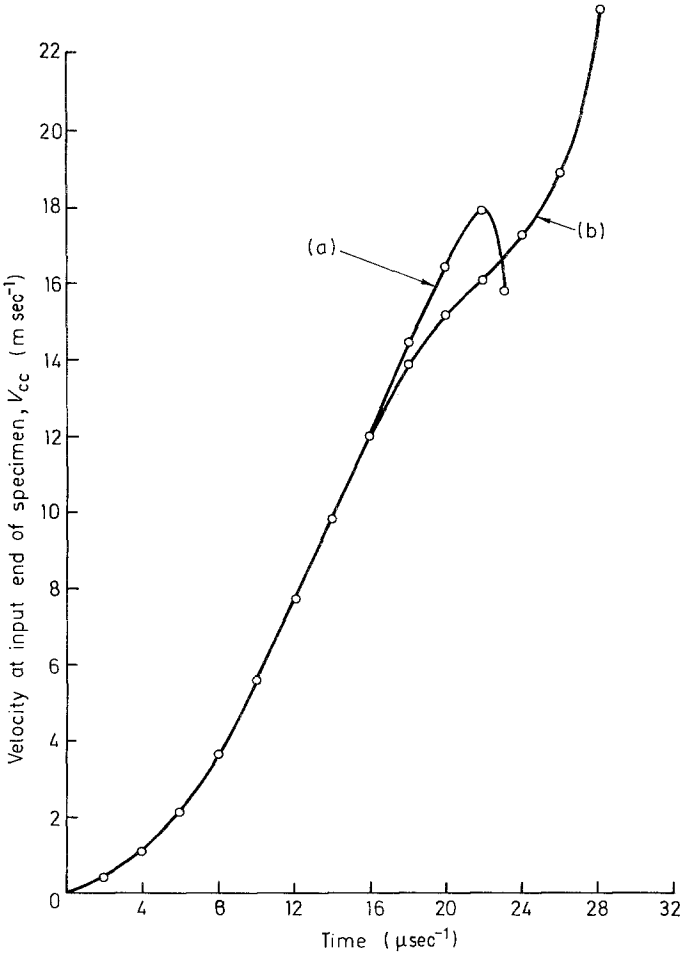

Figure 8 Estimates of velocity V_{cc} at input end of specimen. (a) Derived from inertia bar gauges, station III. (b) Derived from input bar gauges, stations I and II.

stress–strain response in a material as relatively rate insensitive as CFRP.

More importantly the velocity–time curve for V_y obtained in this way greatly exceeds that determined by the traditional technique, i.e. involving a separate elastic test. Using this latter technique gives the stress–strain curve of Fig. 9b for which the apparent modulus is 390 GPa. It should be noted that these large discrepancies between the two estimates for V_y will only appear during the steeply rising region of the velocity profile where small differences in the experimental arrangement and in the acoustic impedance of the components involved will be of major significance. Subsequently the yoke velocity will be dependent almost entirely on the response of the weighbar tube and so will be the same for both elastic and specimen tests. For this reason little weight is given, in general, in tests on ductile metal specimens to strain measurements of less than 1 to 2%. In tests on GFRP, however, since strains of this order are a significant part of the total strain to fracture, it is necessary to use the yoke velocity estimated from CFRP tests over the rising part of the velocity profile and that from the elastic test only in the determination of the subsequent region of the stress–strain curve. In effect, the elastic part of the CFRP specimen test is being used as a more accurate version of the standard separate elastic test.

6.2. Validation of technique for GFRP specimens

Tests were performed at an impact velocity of about 15 msec^{-1} on GFRP specimens oriented with the tensile axis parallel to one of the directions of weave (0° specimens). Strain gauges attached directly to the gauge section of one such specimen failed at just over 1% strain and at a stress, determined from the inertia bar gauges, of 455 MPa. Up to this point the specimen response had been linear, corresponding to a modulus of 44.5 GPa. This compares with a modulus of 46 GPa obtained in the same test using the Hop-

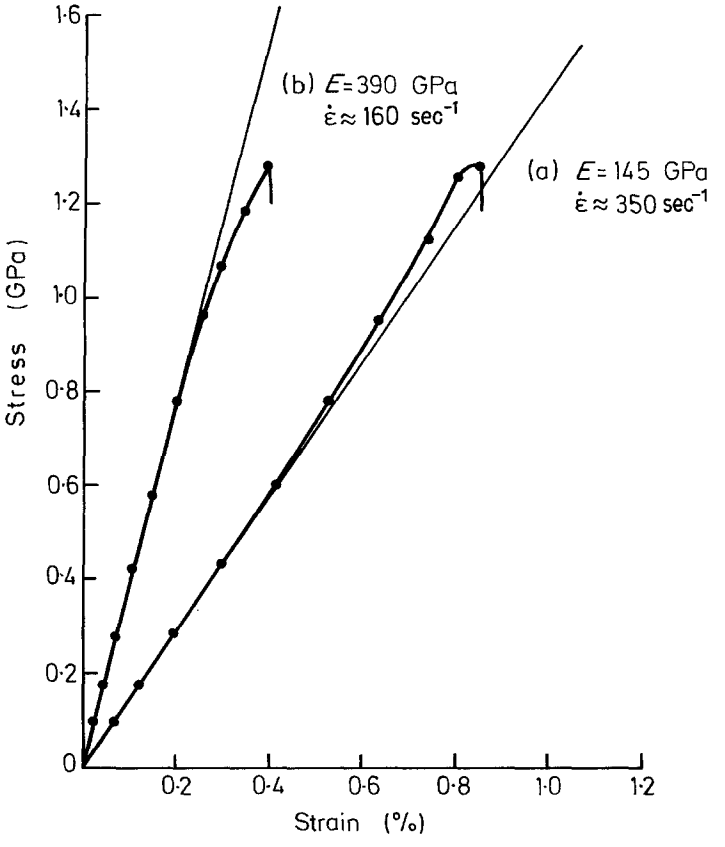

Figure 9 Comparison of stress–strain curves for CFRP obtained on test arrangement of Fig. 1c. (a) Using strain gauges attached to specimen. (b) Using separate "elastic" test.

kinson bar analysis to determine strain and a yoke velocity derived from a CFRP elastic test as described above. The resulting dynamic stress–strain curve is shown in Fig. 10. The close agreement between these two values of modulus encourages confidence in the validity of the technique. Some uncertainty remains, however, at higher strains, beyond the fracture strain of the CFRP specimen and the failure strain of the specimen gauges in the GFRP test. In this region the true yoke velocity is assumed to converge towards that derived from the standard elastic test, see Fig. 11. Extreme choices for the extrapolated curve in Fig. 11 could lead to a range in the calculated fracture strain in Fig. 10 of from 2.85 to 3.25%, i.e. a scatter band of ±7%. In tests on 45° GFRP specimens the same range will apply but the fracture strain is so much higher, about 11%, that the percentage error falls to about ±2%.

7. Tests at low and intermediate rates of strain

In order to determine the effect of strain rate on the tensile deformation and failure of the CFRP and GFRP materials tests were also performed on the same designs of specimen in an Instron loading machine at a rate of about 10^{-4} sec^{-1} and in an hydraulically-operated loading machine [21] at a rate of about $10\,sec^{-1}$. For both machines and for each specimen material, calibration tests for the elastic deflection of the testing machine were performed using strain gauges attached directly to the specimen gauge region. Results for one such test at the intermediate rate, on a CFRP specimen, are given in Fig. 12. Signals showing the variation with time of the specimen strain, ϵ_s (from strain gauges attached to the specimen), the applied load P (from the load cell strain gauges) and the total deflection, δ of specimen and machine (from transducers attached to the moving crosshead) were stored in a transient recorder and subsequently displayed on an oscilloscope screen using both the y–t and the x–y mode. In the latter an essentially linear dependence of load both on strain and on total deflection is observed.

8. Results

8.1 Stress–strain response

Stress–strain curves for CFRP specimens at three

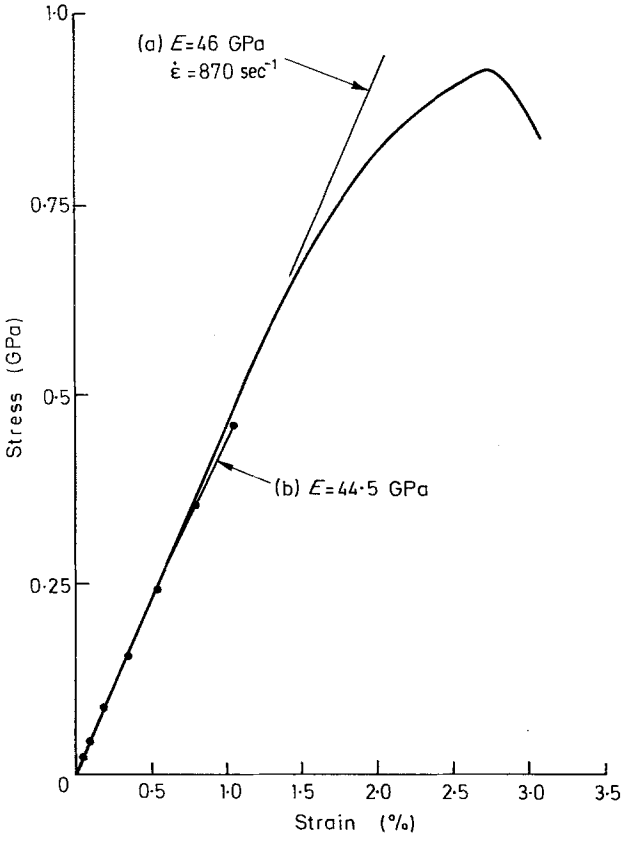

Figure 10 Tensile stress–strain curve for 0° GFRP specimen (impact velocity, 15 msec^{-1}) (a) specimen strain determined by Hopkinson-bar analysis; (b) specimen strain determined from strain gauges attached to specimen.

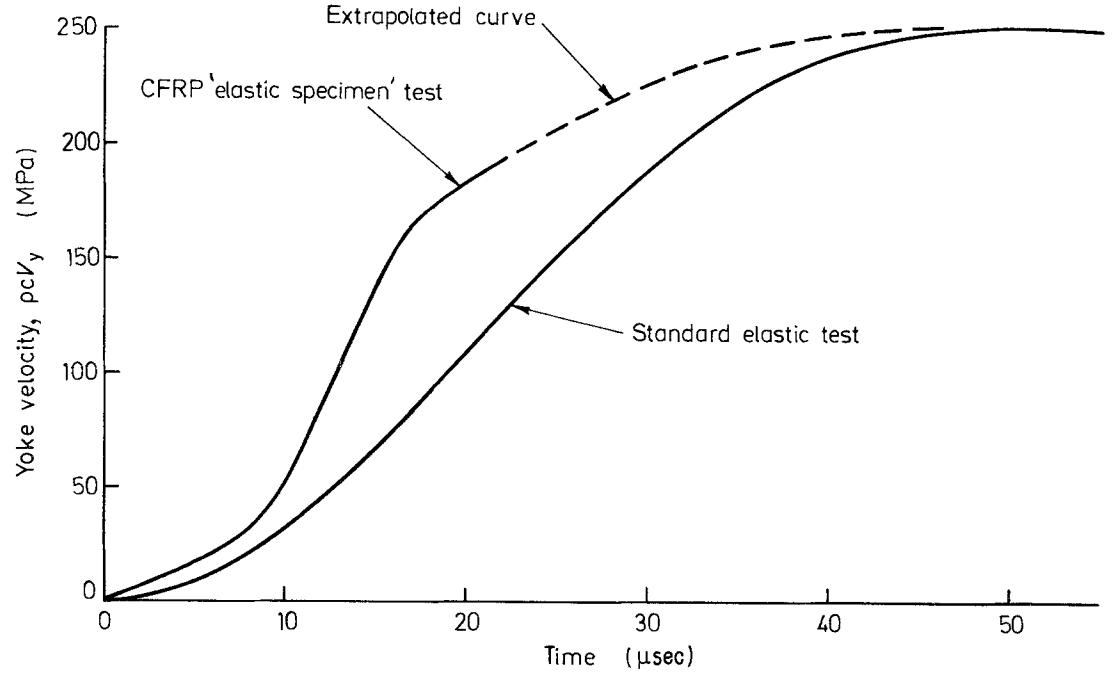

Figure 11 Comparison of Yoke Velocities determined from standard elastic test and from CFRP elastic specimen test (impact velocity, 10 msec^{-1}).

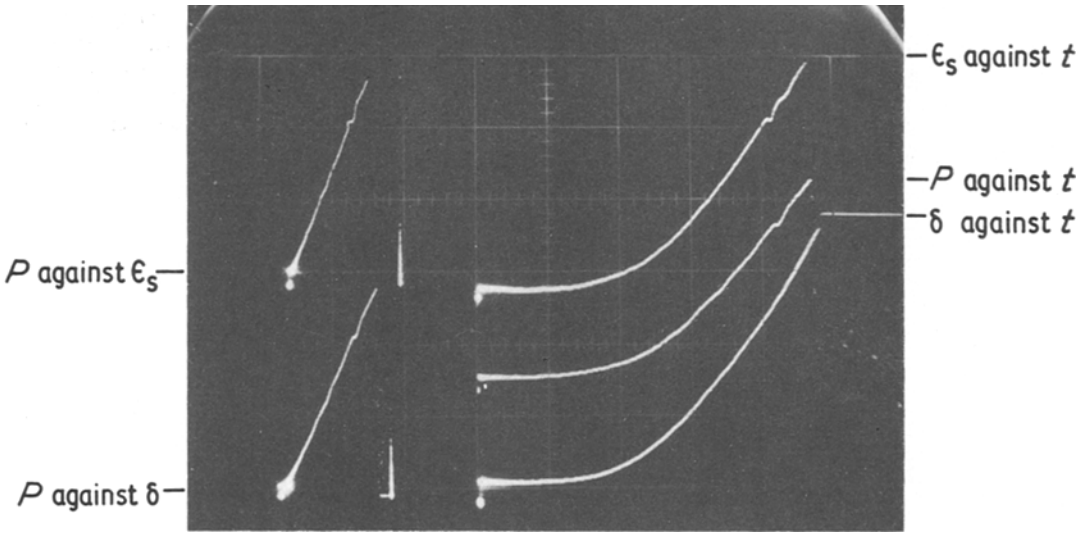

Figure 12 Test records at an intermediate rate of strain (CFRP specimen; strain rate about 7 sec^{-1}). (a) Load, P, against specimen strain, ϵ_s. (b) Load, P, against total deflection, δ. (c) Specimen strain, ϵ_s, against time, t. (d) Load, P, against time, t. (e) Total deflection, δ, against time, t.

rates of strain are presented in Fig. 13. The full line and the quoted values of strain rate and modulus were derived in each case from a test in which strain gauges were attached directly to the specimen. The scatter bands refer to data from further tests without strain gauges on the specimen. Similar results for 0° and 45° GRFP specimens are presented in Figs. 14 and 15. A significantly different behaviour is shown by the two types of material. For CFRP specimens over nearly seven orders of magnitude, no effect of strain rate could be detected on either the tensile modulus, 146 ± 6 GPa, or the stress at fracture, 1.2 ± 0.1 GPa. In contrast, for both orientations of GFRP specimen the maximum stress preceding failure increased dramatically with strain rate, from 348 ± 35 MPa at 10^{-4} sec^{-1} to 899 ± 28 MPa at 870 sec^{-1} for 0° specimens and from 212 ± 12 MPa at 2.5×10^{-4} sec^{-1} to 392 ± 38 MPa at 1120 sec^{-1} for the 45° specimens. Also, in the 0° specimens a marked effect of strain rate was apparent on the modulus, which increased from 19.6 ± 0.9 GPa to 48.6 ± 2.9 GPa over the same range of strain rate. For these specimens the stress–strain response becomes increasingly nonlinear with increasing strain rate and the strain at fracture increases from about 2% to about 3%. The 45° specimens also show an increase in modulus with increasing strain rate but the effect is less marked and of the same order as the accuracy of measurement. The initial linear range, however, increases significantly with increasing strain rate as also does the strain at failure, from about 7.5% at the lowest rate to about 11.5% under impact loading.

8.2 Fracture appearance

For the CFRP specimens, a similar fracture mode, i.e. a tensile failure in the centre of the parallel gauge region with little damage to either side of the fracture surface, see Fig. 16a, was found at all strain rates. In contrast, a marked change in fracture appearance with strain rate was observed in tests on 0° GFRP specimens. At quasi-static rates, see Fig. 16b, damage was limited to regions close to the fracture surface. At increasing rates the damage was found to extend further from the fracture surface, covering the entire gauge region, i.e. well beyond the 6 mm parallel section, in tests at impact rates, see Fig. 16c. In tests on 45° GFRP specimens the damage covers the entire gauge region at all rates of strain. In general the fracture surface followed steps inclined at 45° to the direction of loading. Differences between individual specimens were observed but appeared to be unrelated to the rate of straining.

9. Discussion

9.1. CFRP material

As far as is known no other directly comparable data on the tensile impact behaviour of unidirectionally-reinforced CFRP are available. Similar tests, but on carbon/epoxy specimens with a

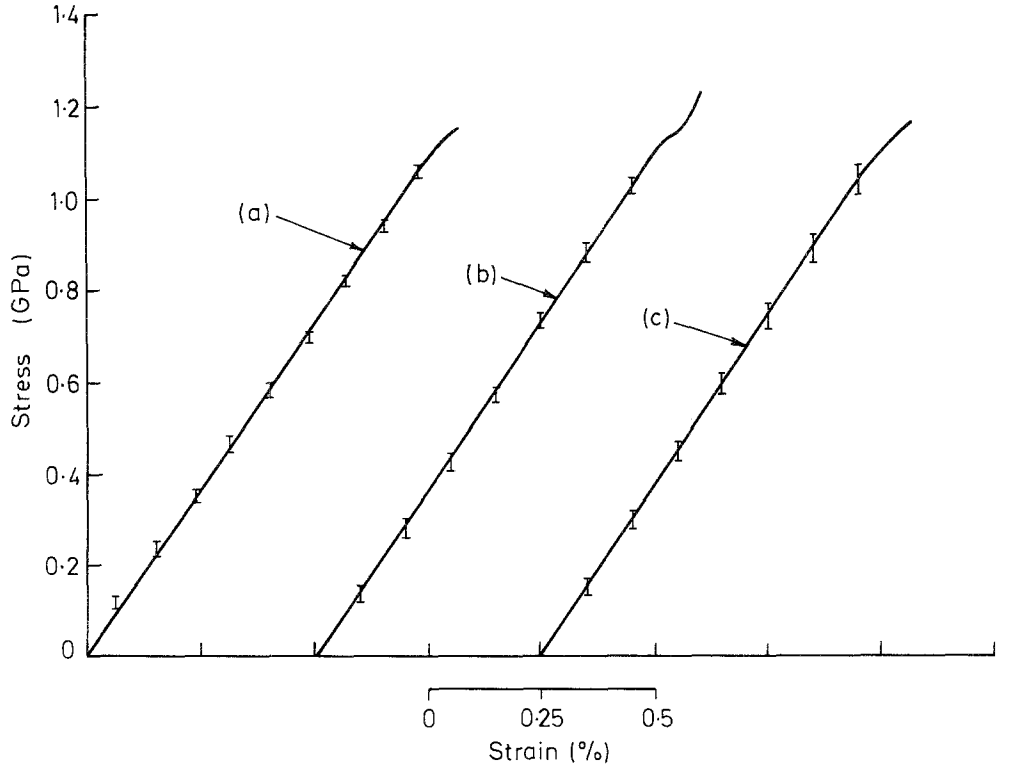

Figure 13 Tensile stress–strain curves for CFRP specimens (a) $\dot{\epsilon} = 5 \times 10^{-4}$ sec^{-1}, $E = 145$ GPa, $\sigma_f = 1.21 \pm 0.07$ GPa (mean of 5 tests). (b) $\dot{\epsilon} = 7$ sec^{-1}, $E = 145$ GPa, $\sigma_f = 1.26 \pm 0.07$ GPa (mean of 4 tests). (c) $\dot{\epsilon} = 450$ sec^{-1}, $E = 149$ GPa, $\sigma_f = 1.14 \pm 0.05$ GPa (mean of 4 tests).

plain-woven cloth reinforcement, were performed by Kawata *et al.* [16]. They also found the mechanical response to be relatively insensitive to strain rate. Impact tests on unidirectionally-reinforced CFRP, but in compression, were performed by Griffiths and Martin [9]. Although they reported a dynamic modulus significantly higher than the generally quoted static moduli for the same class of material specimen geometry was shown to affect the shape of their dynamic stress–strain curves so some doubt must remain regarding the validity of their results.

An anomaly is also apparent in the present CFRP results. Stress–strain curves obtained at an impact velocity of 10 msec^{-1}, using both the modified tensile SHPB (with and without strain gauges on the specimen, see Fig. 6) and the original version of tensile SHPB (also with strain gauges on the specimen, see Fig. 9) show a slight increase in stiffness just before failure. This effect was not apparent, however, at lower rates or at an impact velocity of 15 msec^{-1}, see Fig. 13, even in tests where strain gauges attached to the specimen monitored the specimen strain. An explanation of this difference in behaviour is not immediately apparent, nor is it clear whether it is of any real significance.

9.2. GFRP material

Because of the different reinforcement geometry, a direct comparison with the present CFRP results is not possible. Tensile tests on glass/epoxy specimens with a fine-wave reinforcement have previously been performed, at intermediate loading rates by Pink and Campbell [22] and at impact rates by Kawata *et al.* [16]. The strain-rate sensitivities of the fracture stress and the fracture strain obtained in these two investigations are compared with the present results in Figs. 17 and 18. Kawata tested 0° specimens at only two strain rates. Pink and Campbell tested both 0° and 45° specimens cut from similar "Permaglass 22FE" plate (0.9 mm thick with five layers of fine-weave glass cloth) to that used in the present investigation at some ten or more strain rates over the range 10^{-4} to 10 sec^{-1}. Over this strain rate range their results show the same general trends as found here. The discrepancy in absolute values of fracture

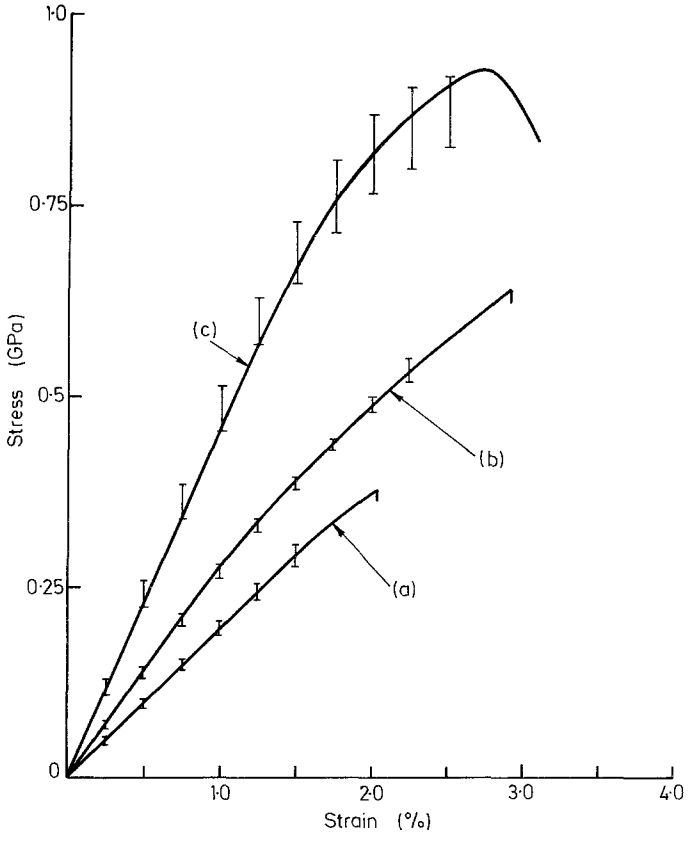

Figure 14 Tensile stress–strain curves for 0° GFRP specimens. (a) $\dot{\epsilon} = 10^{-4}$ sec^{-1}, $E = 19.6$ GPa, $\sigma_{max} = 348 \pm 35$ MPa (mean of 5 tests). (b) $\dot{\epsilon} = 23$ sec^{-1}, $E = 28$ GPa, $\sigma_{max} = 592 \pm 54$ MPa (mean of 5 tests). (c) $\dot{\epsilon} = 870$ sec^{-1}, $E = 46$ GPa, $\sigma_{max} = 899 \pm 28$ MPa (mean of 4 tests).

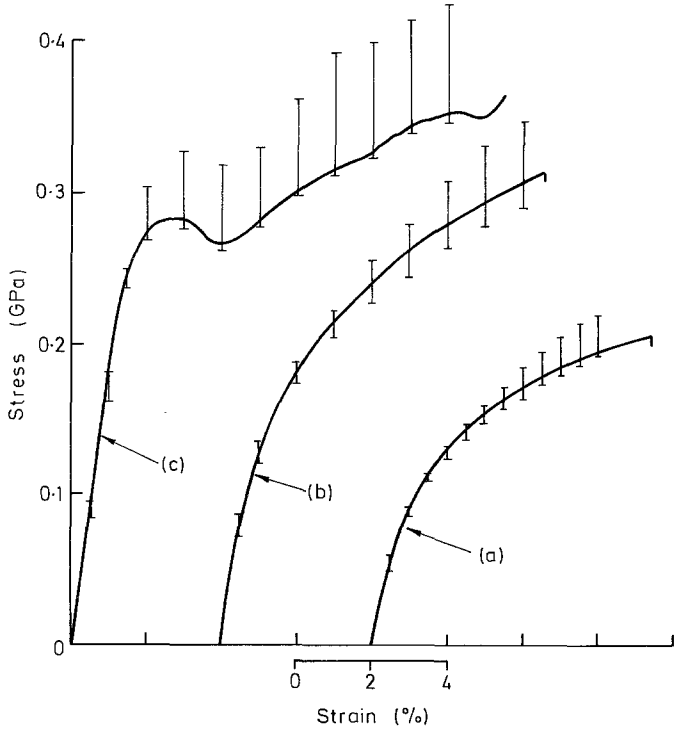

Figure 15 Tensile stress–strain curves for 45° GFRP specimens. (a) $\dot{\epsilon} = 2.5 \times 10^{-4}$ sec^{-1}, $E = 11.3$ GPa, $\sigma_{max} = 212 \pm 12$ MPa (mean of 5 tests). (b) $\dot{\epsilon} = 24$ sec^{-1}, $E = 15.0$ GPa, $\sigma_{max} = 325 \pm 26$ MPa (mean of 4 tests). (c) $\dot{\epsilon} = 1120$ sec^{-1}, $E = 18.3$ GPa, $\sigma_{max} = 392 \pm 38$ MPa (mean of 5 tests).

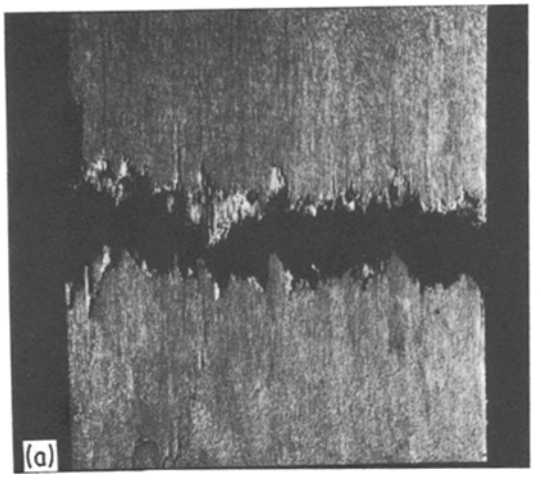

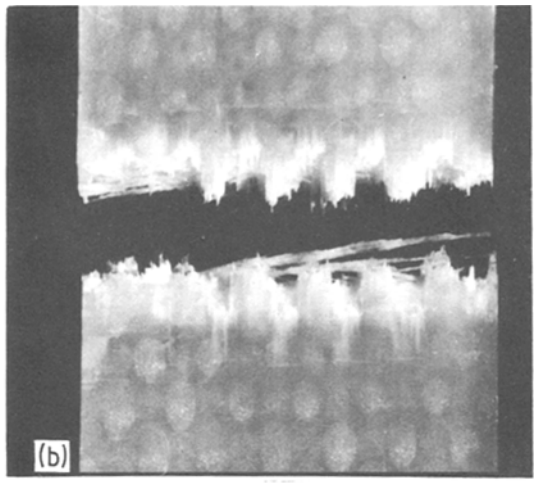

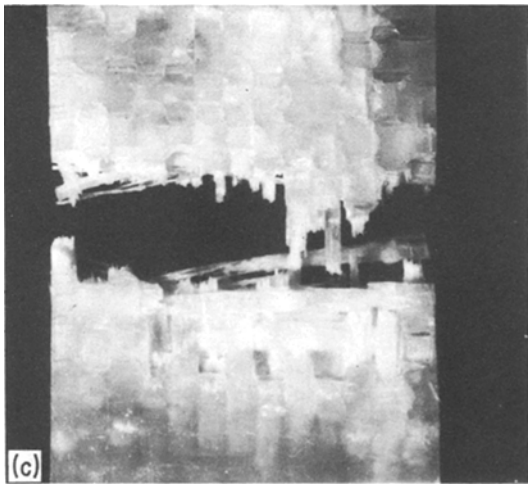

Figure 16 Fracture appearance of composite specimens (a) CFRP specimen after straining at a mean rate of $450\,sec^{-1}$ (× 8), (b) 0° GFRP specimen after straining at a mean rate of $10^{-4}\,sec^{-1}$ (× 8) and (c) 0° GFRP specimen after straining at a mean rate of $870\,sec^{-1}$ (× 7.5).

stress and strain, their results being consistently lower than those reported here, may arise from the different designs of specimen used or from differences between the plates from which the specimens were cut. The results of Kawata *et al.* [16] under impact loading do not show such a dramatic increase in fracture stress as here but indicate a very much higher strain to fracture. Both these discrepancies could be connected with the loading arrangement used by Kawata *et al.*, in that the development of significant bending stresses on impact could lead to an apparent reduction in the tensile load at failure while the use of a cylindrical specimen with a screw fixing makes the accurate determination of small specimen strains by the Hopkinson-bar analysis very difficult.

9.3. Fracture behaviour

Despite these discrepancies between the dynamic fracture stresses and fracture strains determined here and in the work of Kawata *et al.* [16], in both investigations the same effect of strain rate on fracture appearance was obtained. In all tests on CFRP and in quasi-static tests on 0° specimens of GFRP damage is confined to regions close to the fracture plane while in impact tests on GFRP, damage covers much of the gauge region and the reinforcement separates from the matrix over a considerable distance to either side of the fracture surface. It is also apparent, see Fig. 14, that the initial modulus increases with strain rate and at higher loads the stress–strain curve becomes increasingly nonlinear. In consequence the energy absorbed in fracturing the GFRP specimens, as determined from the area under the stress–strain curve, increases dramatically with strain rate, see Table I, whereas that for the CFRP specimens remains unaffected by the strain rate and is significantly less than that obtained for the GFRP specimens at intermediate and impact rates of

TABLE I Energy absorbed to fracture per unit volume of specimen (MPa)

Strain rate	Material		
	CFRP	GFRP	
		0° specimens	45° specimens
Low rate	4.6	4.1	11.3
Intermediate rate	5.3	10.5	19.8
Impact rate	5.0	18.5	32.9

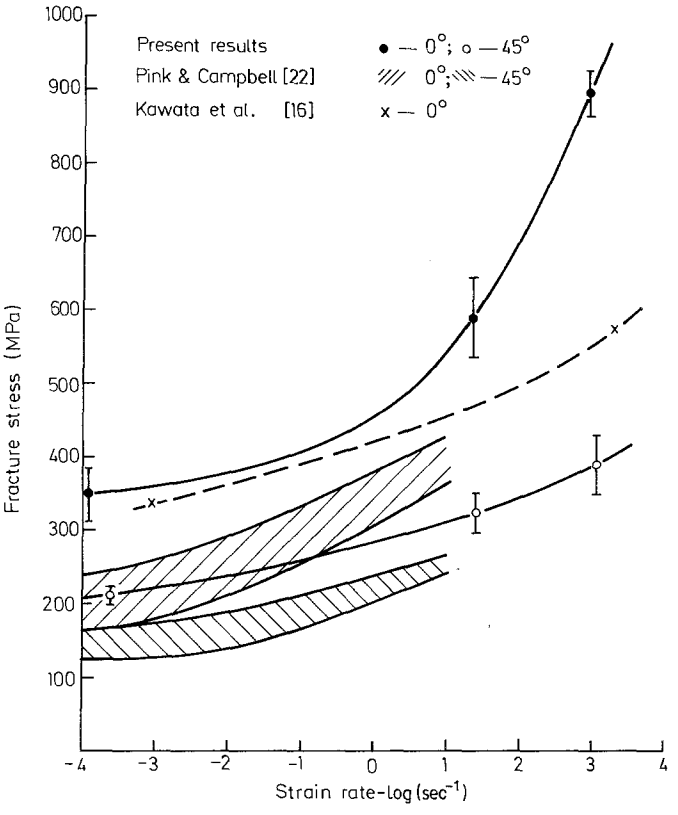

Figure 17 Effect of strain rate on maximum stress in GFRP specimens.

strain, although a direct comparison is clearly invalid because of the different reinforcement geometries.

This marked difference between the impact response of carbon/epoxy composites and glass/epoxy composites has been known for some time [7] and has lead to the introduction of hybrid composites where the high "toughness" of GFRP at impact rates is combined with the high stiffness of CFRP at all rates in an attempt to opimize the overall mechanical behaviour. Most studies of the impact response of hybrid composites, however, have employed Charpy type tests on notched [23] or un-notched [24] specimens. Even though an instrumented tup may be used [5] and a load–time history obtained, the Charpy technique suffers serious limitations when fundamental information on the impact response is being sought so it is not surprising that conflicting results have sometimes been obtained [4, 25]. The present testing technique, however, avoids many of these limitations and should, therefore, allow a more fundamental study to be made of the impact response of composites in general and hybrids in particular.

9.4 Testing technique

As discussed above, the technique developed here for tensile impact testing of composite materials is either limited to specimens failing within about 30 μsec or requires very careful determination of the input velocity. Although it has proved possible to calibrate for the input velocity, using the previously determined response of CFRP specimens, with sufficient accuracy to permit the testing of GFRP specimens to failure at times up to about 100 μsec, nevertheless it would clearly be more satisfactory to monitor input and output stress and velocity in the same test. The construction of an extended version of the modified tensile SHPB to allow this for times up to about 150 μsec is now in hand.

A second limitation relates to the testing of commercially-produced (high volume fraction) unidirectionally-reinforced GFRP where, using the same design of specimen as for CFRP, it has not as yet proved possible to obtain a tensile failure in the specimen gauge region. Instead failure always occurs in shear within the specimen at the resin/fibre interface nearest to the slots in the loading bars. The use of the instrumented

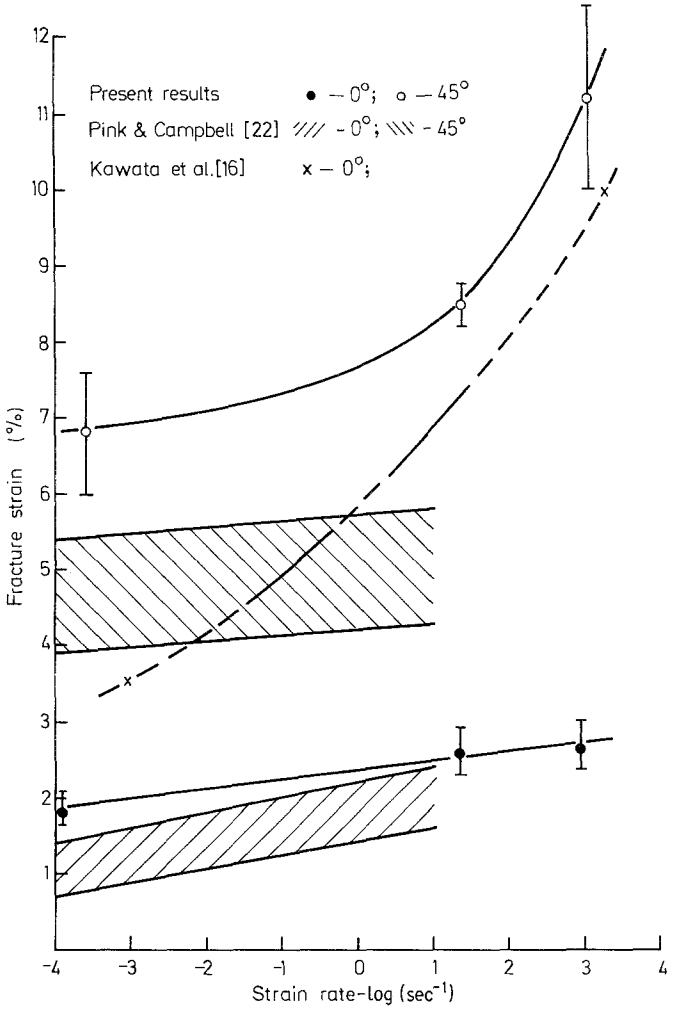

Figure 18 Effect of strain rate on fracture strain in GFRP specimens.

input bar in the extended version of the present impact tester will be required to monitor the effects of any changes in specimen design necessary in the solution of this problem.

10. Conclusions

A modified version of the tensile SHPB apparatus has been successfully developed for the tensile impact testing of unidirectionally-reinforced CFRP. Stress equilibrium across the specimen is attained at an early stage in the test. Specimen strain is determined to an accuracy of about ± 3% and the tensile modulus to about ± 5%. The technique has been successfully extended to the testing of GFRP specimens having a woven-roving reinforcement with the tensile axes parallel to, or at 45° to, the principal reinforcement directions.

Over a range from about 10^{-4} sec^{-1} to about 1000 sec^{-1} the modulus, fracture strength and failure mode of unidirectionally-reinforced CFRP are found to be independent of strain rate. In contrast both orientations of GFRP specimen showed a dramatic increase in failure strength at impact rates of strain, a significant increase in failure strain and, for the 0° specimens, a marked increase in initial modulus. The change in mechanical response with increasing strain rate was associated, in the 0° specimens, with a change in the fracture appearance, limited matrix cracking close to the fracture surface at low rates extending to cover the entire gauge section at impact rates where extensive debonding between the fibres and the matrix was also observed.

References

1. G. DOREY, "Fracture behaviour of carbon fibre composites subjected to impact loads", AGARD Conference Proceedings 163 on Failure modes of composite materials with organic matrices and their consequences in design. AGARD-CP-163, 1974.

2. A. E. ARMÉNAKAS and C. A. SCIAMMARELLA, *Exp. Mech.* 13 (1973) 433.
3. A. ROTEM and J. M. LIFSHITZ, in Proceedings of the 26th Annual Technical Conference, SPI Reinforced Plastics/Composites Division (Society of Plastics Industry, New York, 1971) Paper 10-G.
4. G. MAROM, S. FISCHER, F. R. TULER and H. D. WAGNER, *J. Mater. Sci.* 13 (1978) 1419.
5. D. F. ADAMS and A. K. MILLER, *ibid.* 11 (1976) 1697.
6. M. G. PHILLIPS, "Fracture and fatigue of hybrid composites", in Fibre Composite Hybrid Materials, edited by N. L. Hancox (Applied Science Publishers, Barking, Essex, 1981) Chap. 4.
7. D. F. ADAMS, ASTM STP 617 (1977) p. 409.
8. R. L. SIERAKOWSKI, G. E. NEVILL, C. A. ROSS and E. R. JONES, *J. Comp. Mater.* 5 (1971) 362.
9. L. J. GRIFFITHS and D. J. MARTIN, *J. Phys. D. Appl. Phys.* 7 (1974) 2329.
10. T. PARRY and J. HARDING, Colloque International du CNRS No. 139, Plastic behaviour of anisotropic solids, Grenoble, June 1981 (OUEL Report No. 1365/81).
11. J. HARDING, in Proceedings of the Conference on Mechanical Properties at High Rates of Strain, Oxford, April 1979, edited by J. Harding, Conf. Ser. No. 47 (Institute of Physics, Bristol and London, 1979) p. 318.
12. E. McABEE and M. CHMURA, in Proceedings of the 16th Annual Technical Conference, SPI Reinforced Plastics Division, Chicago (Society of Plastics Industry, New York, 1961) Paper 13-D.
13. B. REVSIN and S. R. BODNER, *Israel J. Tech.* 7 (1969) 485.
14. T. FUJII and M. MIKI, in Proceedings of the Symposium on Mechanical Behaviour of Materials, Kyoto, Japan, 1973, p. 83.
15. I. M. DANIEL, R. H. LA BEDZ and T. LIBER, *Exper. Mech.* 21 (1981) 71.
16. K. KAWATA, A. HONDO, S. HASHIMOTO, N. TAKEDA and H. L. CHUNG, in Proceedings of the Japan – US Conference on Composite Materials, Tokyo, January 1981, edited by K. Kawata and T. Akasaka (Japan Society for Composite Materials, Tokyo, 1981) p. 2.
17. J. HARDING and L. M. WELSH, presented at the 4th International Conference on Composite Materials, Tokyo, October 1982 (Japan Society for Composite Materials).
18. P. D. EWINS, RAE Technical Report No. 71217 (1971).
19. "Grafil test methods", Courtaulds Ltd., Carbon Fibres Unit, PO Box 16, Coventry, 1977.
20. J. HARDING, E. O. WOOD and J. D. CAMPBELL, *J. Mech. Eng. Sci.* 2 (1960) 88.
21. R. H. COOPER and J. D. CAMPBELL, *ibid.* 9 (1967) 278.
22. E. PINK and J. D. CAMPBELL, *J. Mater. Sci.* 9 (1974) 658.
23. D. F. ADAMS, *ibid.* 10 (1975) 1591.
24. R. R. DIXON, 35th SPE Conference, USA (1977) p. 344.
25. B. HARRIS and A. R. BUNSELL, *Composites* 6 (1975) 197.

Received 1 October
and accepted 23 November 1982